Theoretical Chemistry Accounts (2021) 140:83
https://doi.org/10.1007/s00214-021-02789-y

REGULAR ARTICLE

A molecular electron density theory study of the [3 + 2] cycloaddition reaction of nitronic ester with methyl acrylate

Haydar A. Mohammad-Salim[1]

Received: 7 December 2020 / Accepted: 28 May 2021 / Published online: 9 June 2021

Abstract

The [3 + 2] cycloaddition (32CA) reaction of nitronic ester with methyl acrylate has been studied within the molecular electron density theory to analyse the mechanism and experimentally observed regioselectivity. Electron localisation function (ELF) study predicts zwitter-ionic character of the nitrone, allowing its participation in *zw*-type 32CA reactions associated with high energy barrier demanding overcome through appropriate electrophilic–nucleophilic interactions. Analysis of the CDFT indices predict the global electronic flux from the strong nucleophilic nitrone to the electrophilic methyl acrylate. These 32CA reactions are exergonic with negative reactions Gibbs free energies along *ortho* regiochemical pathway. Among the *ortho* and *meta* regiochemical pathways, *ortho path* is preferred owing to the higher thermodynamic stability of the cycloadducts. Bonding evolution theory (BET) study predicts *one-step* mechanism with early transition states for the *ortho* and *meta* pathways, in conformity with the ELF topological study at the transition states.

Keywords Molecular electron density theory · [3 + 2] Cycloaddition reactions · Regioselectivity · Electron localisation function · Conceptual DFT

1 Introduction

Since the last two decades, computational chemistry has emerged as an important tool to analyse the experimentally observed reactivity and selectivity outcomes by developing a systematic outline of the mechanism of chemical reactions [1]. However, in spite of the ever-increasing modern applications of the computational science in chemistry, the underlying theories of organic chemistry had not experienced major breakthrough since last 40 years, until in 2016 Domingo proposed the molecular electron density theory (MEDT) to recognise the decisive role of electron density changes in the molecular reactivity [2, 3]. Since last 4 years, MEDT has successfully analysed the experimental outcome of several 32CA reactions [3–5]. Recently, we have applied the MEDT concept to analyse the experimental outcome of strain promoted and catalysed 32CA reactions and the observed chemo-, regio- and stereoselectivite synthesis of spiroisoxazolines [6–10].

✉ Haydar A. Mohammad-Salim
hayder.salim@uoz.edu.krd

[1] Department of Chemistry, University of Zakho, Duhok 42001, Iraq

Within the MEDT framework, the three atom components (TACs) participating in the 32CA reactions are classified by characterising their electronic structure, into *pseudodiradical*, *pseudo*(mono)*radical*, carbenoid and zwitter-ionic type, which enables their respective participation in *pdr*- type, *pmr*-type, *cb*-type and *zw*-type 32CA reactions [3, 4]. These 32CA reactions show different reactivity profiles; the *pdr*-type 32CA reactions are associated with lower energy barrier and take place easily, while the *zw*-type 32CA reactions show high energy barrier, demanding overcome through electrophilic–nucleophilic interaction between the reactants [9].

Herein, we present an MEDT study at the B3LYP/6–311 + + G(d,p) level for 32CA reactions of a nitronic ester **1** with methyl acrylate **2**, experimentally realised by Sato and co-workers (see Scheme 1) [11]. However, experimental study by Sato and co-workers has not addressed the mechanistic differences in the feasible reaction paths and the role of electron density flux on the 32CA reaction.

This research work presents the MEDT study in five sections, 3.1 to 3.5 (i) In Sect. 3.1, the topological analysis of the electron localisation function (ELF) at the ground state structures of the reagents **1** and **2** is performed to represent

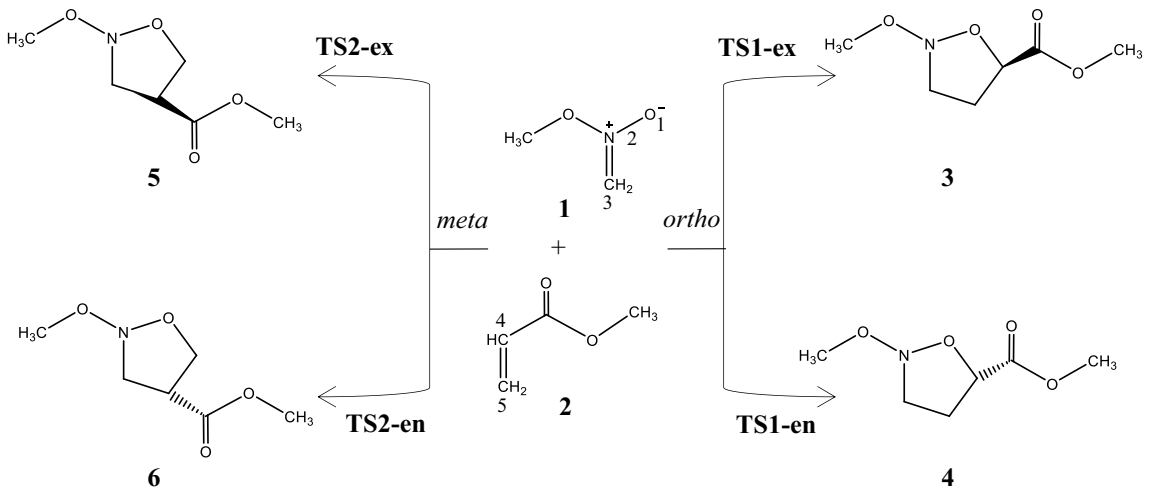

Scheme 1 32CA reaction of nitronic ester 1 with methyl acrylate 2

their electronic structure and consequently to assess their reactivity in 32CA reactions [12, 13]. (ii) In Sect. 3.2, reactivity indices defined within the conceptual density functional theory (CDFT) are analysed to comprehend the polarity of the 32CA reactions [14, 15]. (iii) In Sect. 3.3., potential energy surfaces (PES) along the feasible regioisomeric channels of the 32CA reactions is studied to predict the energy profiles and the global electron density transfer (GEDT) is calculated at the TSs [16, 17]. (iv) In Sect. 3.4, the conjunction of ELF with Thom's catastrophe, namely the bonding evolution theory (BET) proposed by Krokidis is used to structure the mechanism for electron density changes along the regioisomeric paths [12, 13, 18, 19]. (v) In Sect. 3.5, the ELF of the located TSs is analysed.

2 Computational methods

Gaussian 16 package has been used for all calculations [20]. The Berny analytical gradient optimisation method was employed at the B3LYP/6–311 + + G(d,p) level for the optimisation of the stationary points along the potential energy surface of the 32CA reactions [21, 22]. The use of B3LYP functional has been justified as a reliable and accurate method in the analysis of several recent cycloaddition reactions [23–29].

Frequency calculations at the optimised TSs confirmed the presence of one imaginary frequency, while the absence of imaginary frequency was verified for the local minimum. Intrinsic Reaction coordinate (IRC) calculations using Gonzales–Schlegel integration method were carried out to verify the minimum energy reaction pathway connecting the reactants and products via the located TSs [30–32]. Solvent effects in carbon tetrachloride (CCl_4) were considered using polarisable continuum model (PCM) by modelling the solvent using self-consistent reaction field (SCRF) method [33–37].

The CDFT indices are calculated using equations reviewed in Reference 14 and 15 [14, 15]. The global electron density theory (GEDT) at the TSs of each reacting framework was calculated from natural population analysis (NPA) as follows [17, 38, 39]:

$$\text{GEDT (f)} = \sum_{q \in f} q$$

, where q represents the atomic charges, the summation of charges on all atoms in the considered framework represents the GEDT, the positive sign of GEDT indicating global electronic flux from that framework to the other.

Topological analysis of the ELF [12] at the reagents, TSs and IRC points are calculated using Multiwfn software [40] and the isosurfaces are visualised using VMD software [41].

3 Results and discussion

3.1 ELF topological analysis of nitrone 1 and methyl acrylate 2

Under the MEDT framework, a reasonably good correlation has been established between the electronic structure of three atom components (TACs) and their reactivity in 32CA reactions [2–4]. Herein, the ELF of the ground state structures of the reagents **1** and **2** is studied to represent their electronic structures and reactivity in 32CA reactions. Table 1 lists the significant ELF valence basin populations of nitrone **1** and methyl acrylate **2**, while the ELF localisation

Table 1 B3LYP/6–311 + + G(d,p) calculated most significant ELF valence basin populations at 1 and 2

	1	2
V(O1)	3.01	5.60
V'(O1)	2.76	6.15
V(C3,N2)	4.18	
V(N2,O1)	1.55	
V(C4,C5)		1.67
V'(C4,C5)		1.66
V(C5,C6)		2.31

ELF valence basin populations are given in average number of electrons, e

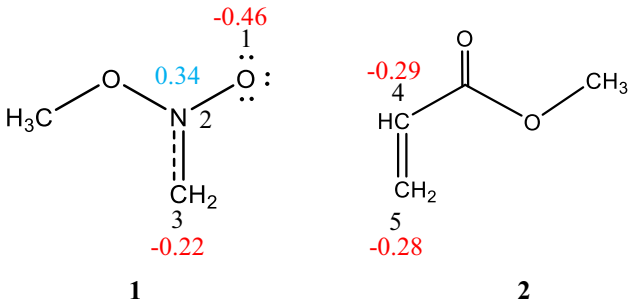

Fig. 2 B3LYP/6–311 + + G(d,p) calculated natural atomic charges, in average number of electrons e, of nitrone **1** and methyl acrylate **2**. Negative charges are coloured in red, and positive charges in blue

domains are shown in Fig. 1. Based on the ELF valence populations, the Lewis structures of the reagents are proposed and are given in Fig. 2.

The ELF of nitrone **1** shows two monosynaptic basins, V(O1) and V'(O1) integrating 5.77 e, one disynaptic basin V(C3,N2) integrating 4.18 e and one disynaptic basin V(N2,O1) integrating 1.55 e, which are associated with the non-bonding electron density on O1 oxygen, underpopulated C3-N2 double bond and underpopulated N2-O1 single bond, respectively.

The ELF of methyl acrylate **2** shows two disynaptic basins for the C4-C5 bonding region with total integrating populations of 3.33 e, associated with the underpopulated C4-C5 double bond, and one disynaptic basin for the C5-C6 bonding region integrating 2.31 e.

After establishing the bonding pattern of the reagents, the atomic charge distribution of nitrone **1** and methyl acrylate **2** was analysed through NPA (Fig. 2) [38, 39]. Oxygen atom O1 of nitrone **1** is negatively charged (−0.46 e) and C3 carbon atom shows charge of −0.22 e, while N2 nitrogen is positively charged (0.34 e). This suggests charge separation in the nitrone although differing from the charges expected by the Lewis's bonding model. Although nitrone **1** is classified as a "zwitterionic" TAC from ELF study, this terminology is not synonymous to the dipolar electronic structure of the nitrones. Instead, it indicates the specific bonding pattern (considering no charges) of the resonance Lewis structure represented by Huisgen for "1,3-dipoles" [42]. In the methyl

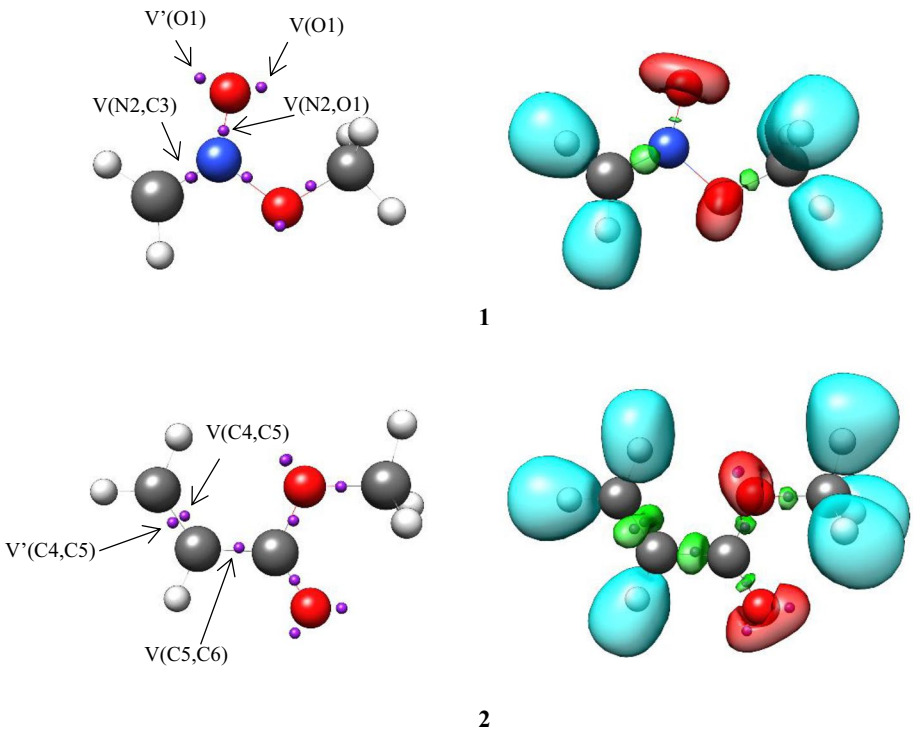

Fig. 1 B3LYP/6–311 + + G(d,p) ELF localisation domains represented at an isosurface value of ELF = 0.82 of nitrone **1** and methyl acrylate **2**. Blue colour represents the protonated basins, green coloured ones are the disynaptic basins, red colour is used to represent the monosynaptic basins. The attractor positions are represented as violet spheres

acrylate **2**, carbon atoms C4 and C5 show negative charge values -0.29 and -0.28.

3.2 Analysis of the CDFT indices of nitrone 1 and methyl acrylate 2

The concept of "*Conceptual DFT*", originated from the pioneering work of Parr, has been utilised in several studies to assess the chemical reactivity of structures participating in 32CA reactions [14, 15, 43–46]. Reactivity indices defined within the conceptual DFT, namely the CDFT indices, have well documented literature and provide an initial comprehension of the molecular reactivity by addressing the chemical behaviour of the reactants [15]. Domingo defined the standard scales for electrophilicity and nucleophilicity indices at the B3LYP/6-31G(d) level, which has therefore been employed herein for the CDFT analysis [47, 48]. Consequently, the CDFT indices, electronic chemical potential, μ, chemical hardness, η, electrophilicity, ω, and nucleophilicity, *N*, at the ground state of nitrone **1** and methyl acrylate **2** are listed in Table 2 [49–52].

The electronic chemical potentials μ of nitrone **1**, $\mu = -3.93$ eV (**1**) is higher than that of methyl acrylate **2** $\mu = -4.80$ eV, suggesting that along the 32CA reaction, the electron density will flux from nitrone **1** to the methyl acrylate **2** [15, 49].

The electrophilicity ω index and the nucleophilicity *N* index of nitrone **1** is 1.38 and 2.75 eV, respectively, being classified as a weak electrophile and a strong nucleophile on the respective scales [47, 48, 51, 52]. The methyl acrylate **2,** with electrophilicty indices $\omega = 2.15$ eV is classified as strong electrophiles and with nucleophilicity indices $N = 1.62$ eV as weak nucleophiles. Consequently, along these *zw*-type 32CA reactions, the methyl acrylate **2** will behave as electrophiles while nitrone **1** will behave as a nucleophile, in conformity with the electronic chemical potentials μ of these species.

Table 2 B3LYP/6-31G(d) CDFT indices of nitrone **1** and methyl acrylate **2**. μ, η, ω and *N* represent electronic chemical potential, chemical hardness, electrophilicity and nucleophilicity indices, respectively, and are expressed in eV

	μ	η	ω	*N*
1	−3.93	5.60	1.38	2.75
2	−4.80	6.15	1.87	1.62

3.3 Analysis of the energy profile associated with the 32CA reactions of nitrone 1 with methyl acrylate 2

Due to non-symmetry of methyl acrylate **2**, two regioisomeric paths, namely the *ortho* and *meta* (see Scheme 1), are feasible for these 32CA reactions. The *ortho* reaction path is associated with the formation of O1-C5 and C3-N4 bonds, while the *meta* channel with the formation of O1-N4 and C3-C5 bonds. The stationary points along these two reactions paths were located and characterised, the reagents, nitrone **1** and methyl acrylate **2**, two TSs for each 32CA reaction, **TS1-ex**, **TS2-en**, **TS3-ex** and **TS4-en** and the corresponding adducts **3**–**6**, respectively, for the 32CA reactions of nitrone **1** with **2**. **TS1-ex** and **TS1-en** correspond to the *ortho* TSs leading to the formation of cycloadducts **3** and **4**, while **TS2-ex** and **TS2-en** are the *meta* TSs leading to the formation of cycloadducts **5** and **6**, respectively. Table 3 lists the relative electronic energies, enthalpies, Gibbs free energies and entropies of the TSs and the cycloadducts.

The energy profile of the 32CA reactions was studied to arrive at some important conclusions (1) These 32CA reactions show negative reaction Gibbs free energies for *ortho* channel, ΔG of -0.28 and −0.18 kcal.mol^{-1} for cycloadducts **3** and **4**, respectively, in gas phase, while only cycloadducts **3** shows negative reaction Gibbs free energy, ΔG of −0.20 kcal.mol^{-1} in CCl_4. These results suggesting exergonic reaction along *ortho* channel, demanding the analysis of the thermodynamic stability of the cycloadducts to predict the preferred regiochemical path. Along the *ortho* channel, the reaction enthalpies are −12.83 (**3**) and −12.35 (**4**) kcal·mol^{-1} in gas phase and −12.50 (**3**) and −11.72 (**4**) kcal·mol^{-1} in CCl_4, while along the *meta* reaction path, the

Table 3 B3LYP/6–311 + + G(d,p) calculated relative energies, enthalpies and Gibbs free energies, in kcal·mol^{-1}, computed at 298 K of the stationary points involved in the 32CA reactions of 32CA reactions of nitrone **1** with methyl acrylate **2**

	Gas phase				CCl_4			
	ΔE	ΔH	ΔG	GEDT	ΔE	ΔH	ΔG	GEDT
TS1-ex	15.30	15.24	27.07	0.07	15.45	15.41	27.12	0.07
3	−12.32	−12.83	−0.28		−12.03	−12.50	−0.20	
TS1 − en	14.56	14.36	27.03	0.14	15.01	14.84	27.4	0.14
4	−11.91	−12.35	−0.18		−11.32	−11.72	0.08	
TS2 − ex	16.80	16.65	28.79	0.03	17.49	17.36	29.45	0.03
5	−11.51	−11.97	0.23		−11.18	−11.64	0.68	
TS2 − en	18.62	18.46	30.61	0.03	19.09	18.94	31.06	0.02
6	−12.22	−12.25	0.06		−11.66	−12.04	0.08	

products show less negative reaction enthalpies −11.97 (**5**) and −12.25 (**6**) kcal·mol^{-1} in gas phase and −11.64 (**5**) and −12.04 (**6**) kcal·mol^{-1} in CCl_4. Thus, the *ortho* adducts show higher relative stability than the *meta* ones owing to their negative reaction enthalpies and lower reaction free energies, suggesting preference for the *ortho* reaction path leading to the formation of cycloadducts **3** and **4**. (2) These 32CA reactions show activation enthalpies between 15.24 (**TS1-ex**) and 14.36 (**TS1-en**) in gas phase and between 15.41 (**TS1-ex**) and 14.84 (**TS1-en**) in CCl_4, in coherence with their *zw*-type classification associated with high activation energies. (3) the inclusion of CCl_4 slightly increases the activation enthalpies due to better solvation of the reagents than the TSs, while the reaction enthalpies are increased in CCl_4 [53].

The B3LYP/6–311 + + G(d,p) optimised geometries of the TSs are given in Fig. 3. In gas phase, the distances between O1 and C5, and C3 and C4 interacting centres at the *ortho* TSs are as follows: 2.37 and 2.04 Å, at **TS1-ex** and 2.51 and 1.96 Å, at **TS-en**, while the distances between O1 and C4, and C3 and C5 interacting centres at the *meta* TSs are: 2.05 and 2.20 Å, at **TS2-ex** and 2.07 and 2.17 Å, at **TS2-en**, respectively. The TSs geometries show similar trend and minimal changes on inclusion of solvent effects in CCl_4. These geometrical parameters imply the extent of bond formation. (1) Considering that the C–O and C–C bond formation begins at the distances of 1.70–1.79 and 1.50–1.70 Å, respectively, these geometrical parameters indicate that at the *ortho* TSs **TS1-ex** and **TS1-en**, the formation of the C–O or C–C single bonds has not yet begun [3]. (2) Considering that the C–C bond formation begins at the distances of 1.90 Å, it is evident that at the *meta* TSs **TS2-ex** and **TS2-en**, the formation of the C–C single covalent bond has not yet started.

Finally, the polar nature of these 32CA reactions was evaluated by the GEDT calculations at the TSs [17]. The gas phase GEDT values at the TSs are 0.07 e at **TS1-ex**, 0.14 e at **TS1-en**, 0.03 e at **TS2-ex**, and 0.03 e at **TS2-en** (see Table 3). In CCl_4, no significant changes occur in the GEDT values at all TSs. The electron density fluxes from nitrone **1** acting as the nucleophile towards methyl acrylate **2** each case, these reactions are classified as forward electron density flux (FEDF), evidenced by the higher nucleophilicity of nitrone **1** relative to the strongly electrophilic methyl acrylate **2** (see Table 2) [54].

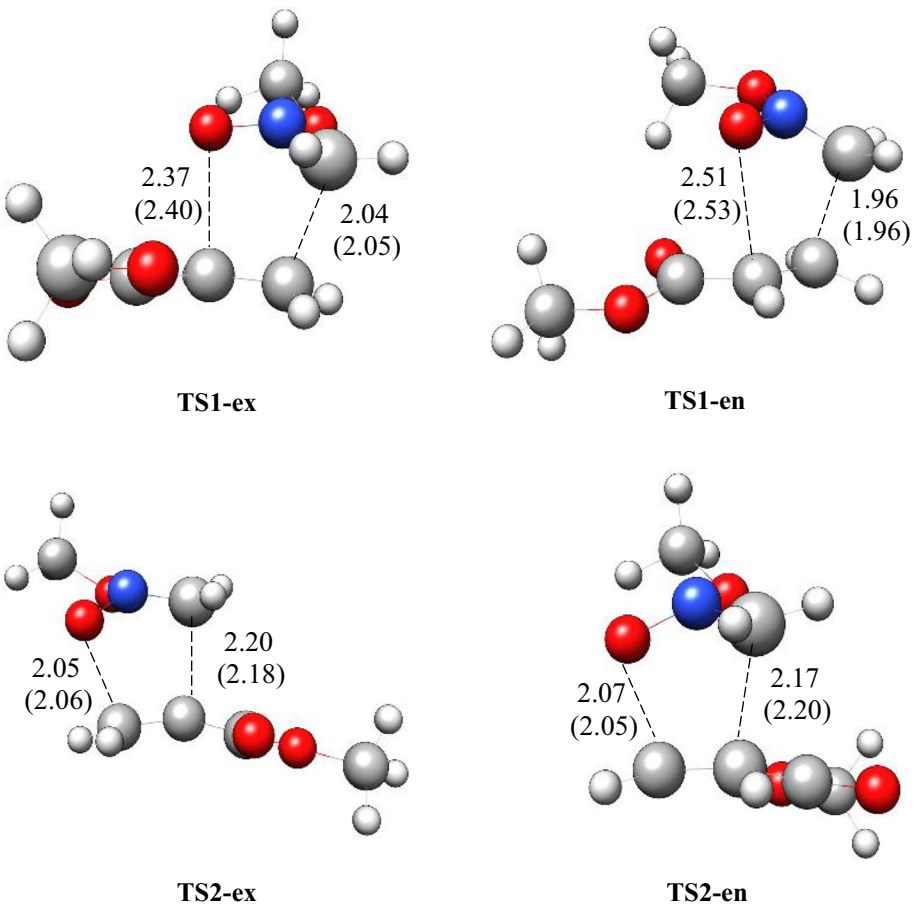

Fig. 3 B3LYP/6–311 + + G(d,p) optimised geometries of TSs involved in the 32CA reactions of nitrone **1** with methyl acrylate **2**. Bond lengths are given in Angstroms. The values in parenthesis are calculated in CCl_4

3.4 Mechanistic implications along the regioisomeric channels of 32CA reaction of nitrone 1 with methyl acrylate 2 from bonding evolution theory (BET) study

The ELF basin populations at the reacting centres for the 32CA reaction of nitrone **1** with methyl acrylate **2** along the *ortho* regioisomeric path in **TS1-ex** are given in Table 4. The identification of catastrophe from ELF basin analysis allows characterising six topological *phases I, II, III, IV, V* and *VI*, identified by the starting points **P1**, **P2**, **P3**, **P4**, **P5** and **P6**, respectively (see Table 4).

The ELF topology of the starting point **P1** shows similar bonding pattern as the individual reagents (see Table 1). At **P2**, (d(C3-C5) = 2.226 Å, d(O1-C4) = 2.642 Å)), the monosynaptic basin V(N2) associated with the N2 nitrogen lone pair integrating 1.15 e is created by deriving electron density from the C3-N2 bonding region experiencing depopulation from 4.17 e at **P1** to 2.88 e at **P2**. This phase also shows the presence of monosynaptic basin V(C3) integrating 0.34 e. Phases *III* is characterised by the creation of *pseudoradical* centres at C3 and C4 at **P3** showing the formation of monosynaptic basins V(C3) and V(C4) integrating 0.55 e and 0.99 e, respectively. Note that C3-N2 bonding region experiences depopulation from 2.88 e at **P2** to 2.49 e at **P3,** while the C4-C5 bonding region experiences depopulation from 3.14 e at **P2** to 2.84 e at **P3**. The transition structure **TS1-ex** belongs to phase *III*. Note that at the **TS1-ex**, the formation of O1-C5 and C3-N4 covalent bonds has not begun. In phase *IV*, identified by the IRC point **P4**, the first C3-C5 single bond formation begins at the C3-C5 distance of 1.718 Å, characterised by the creation of disynaptic basin V(C3, C5) integrating 1.09 e, while in phase *VI*, identified by the IRC point **P6**, the second O1-C4 single bond formation begins at the O1-C4 distance of 1.728 Å, characterised by the creation of disynaptic basin V(O1,C4) integrating 0.74 e. Finally, at the cycloadduct **3**, the molecular geometry is relaxed at O1-C4 and C3-C5 distances of 1.464 and 1.538 Å, respectively.

3.5 ELF topological analysis at the TSs

The ELF valence basin populations at the four TSs, **TS1-ex**, **TS1-en**, **TS2-ex** and **TS2-ex** are listed in Table 5, while the ELF localisation domains are represented in Fig. 4. ELF of the *ortho* TSs, **TS1-ex** and **TS1-en** show the presence of monosynaptic V(N2) integrating 1.56 e and 1.34 e, respectively, which are absent in the ELF of nitrone **1**. ELF of the **TS1-ex** shows the presence of V(C3) and V(C4) monosynaptic basins integrating 0.55 e and 0.99 e, respectively,

Table 5 B3LYP/6–311 + + G(d,p) calculated ELF valence basin populations at the TSs

	TS1-ex	TS1-en	TS2-ex	TS2-en
V(O1)	2.77	2.79	2.82	2.77
V'(O1)	2.92	2.89	2.92	2.95
V(N2)	1.56	1.34	1.75	1.76
V(C3,N2)	2.49	2.56	2.47	2.48
V(N2,O1)	1.42	1.43	1.32	1.31
V(C4,C5)	2.87	2.29	2.81	2.81
V(C3)	0.55	0.95	0.38	0.41
V(C4)	0.99		0.27	0.30

Table 4 ELF valence basin populations of the IRC structures **P1**-**P6** defining the six phases, characterising the molecular mechanism of the *ortho* (**TS1-ex**) reaction path of 32CA reaction of nitrone **1** with methyl acrylate **2**. The distances of the forming bond distances are given in angstrom units, Å

Phases	I	II	III	IV	V	VI	
Structures	P1	P2	P3 TS1-ex	P4	P5	P6	3
d(C3-C5)	2.637	2.226	2.041	1.718	1.653	1.565	1.538
d(O1-C4)	2.642	2.448	2.372	2.221	2.141	1.728	1.464
GEDT	0.04	0.09	0.07	0.05	0.04	0.02	0.04
V(O1)	3.01	2.94	2.92	2.92	2.90	2.74	2.54
V'(O1)	2.76	2.73	2.77	2.76	2.69	2.59	2.49
V(C3,N2)	4.17	2.88	2.49	2.33	2.11	2.05	2.02
V(N2,O1)	1.55	1.44	1.42	1.35	1.32	1.05	0.97
V(N2)		1.15	1.56	1.76	2.02	2.38	2.48
V(C4,C5)	1.67	1.58	2.84	2.65	2.26	2.02	1.93
V'(C4,C5)	1.66	1.56					
V(C5,C6)	2.31						
V(C3)		0.34	0.55				
V(C4)			0.99				
V(C5)					0.11		
V(O1,C4)						0.74	1.22
V(C3,C5)				1.09	1.59	1.76	1.84

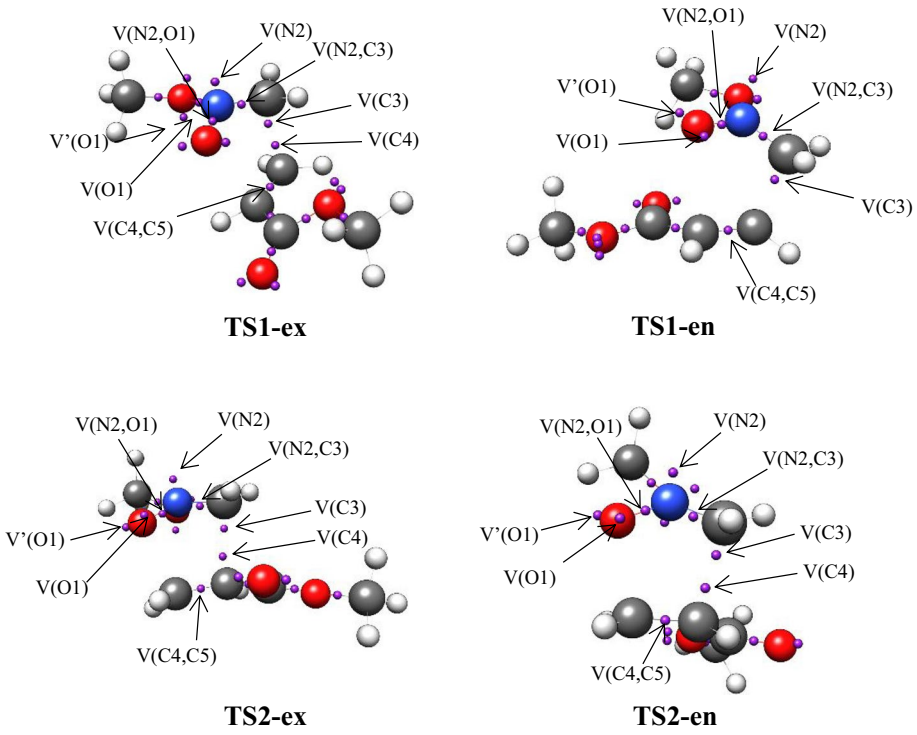

Fig. 4 B3LYP/6–311 + + G(d,p) the ELF attractor positions of TSs involved in the 32CA reactions of nitrone **1** with methyl acrylate **2**

while only V(C3) monosynaptic basin is shown in **TS1-en**. The disynaptic V(C3,N2) basin in nitrone **1** associated with the C3-N2 bonding region integrating 4.18 e in nitrone **1** is depopulated to 2.49 e in **TS1-ex**, 2.56 e in **TS1-en**, 2.47 e in **TS2-ex** and 2.48 e in **TS2-en**. The disynaptic V(C4,C5) and V'(C4,C5) basins in the methyl acrylate **2** associated with the C4-C5 bonding region with total integrating population of 3.33 e is depopulated to 2.87 e in **TS1-ex**, 2.29 e in **TS1-en**, 2.81 e in **TS2-ex** and 2.81 e in **TS2-en**. At the *ortho* and *meta* TSs, the formation of new single covalent bond has not been started.

4 Conclusion

An MEDT study is presented for 32CA reaction of a nitronic ester **1** to methyl acrylate **2** at the B3LYP/6–311 + + G(d,p) computational level. The ELF topological analysis at the ground state structures allow classification of the nitrone **1** as a zwitter-ionic TAC, allowing its participation in *zw*-type 32CA reactions, demanding appropriate electrophilic–nucleophilic interactions.

The global electronic flux from the nitrone **1** to methyl acrylate **2** is predicted, owing to the high electronic chemical potential and strong nucleophilicity of the cyclic nitrone **1** relative to the methyl acrylate **2**, which is confirmed from the GEDT calculations at the located TSs. These 32CA reactions are exergonic with negative free energy of reaction. The cycloadducts **3** and **4** show higher thermodynamic stability relative to the cycloadducts **6** and **5**, suggesting regioselectivity in complete coherence with the experiments.

BET study along the regioisomeric reaction channels allows arriving at some important mechanistic conclusions. Along both the reaction paths, in the first four *phases*, the C=N bonding region of nitrone **1** and C=C bonding region of the methyl acrylate **2** are depopulated to create *pseudoradical* centres at C3, C4 and C5 carbons and lone pair electron density at N2 nitrogen. ELF study at the TSs show early TSs along the *ortho* and *meta* reaction paths, when the formation of new single covalent bond has not been started.

Declarations

Conflict of interest The authors declare no conflict of interest.

References

1. Krylov A, Windus TL, Barnes T, Marin-Rimoldi E, Nash JA, Pritchard B, Smith DGA, Altarawy D, Saxe P, Clementi C, Crawford TD, Harrison RJ, Jha S, Pande VS, Head-Gordon T (2018) Perspective: computational chemistry software and its advancement as illustrated through three grand challenge cases for molecular science. J Chem Phys. https://doi.org/10.1063/1.5052551
2. Domingo LR (2016) Molecular electron density theory: a modern view of reactivity in organic chemistry. Molecules 21(10):1319. https://doi.org/10.3390/molecules21101319

3. Ríos-Gutiérrez M, Domingo LR (2019) Unravelling the mysteries of the [3+2] cycloaddition reactions. Euro J Org Chem 2–3:267–282. https://doi.org/10.1002/ejoc.201800916
4. Domingo LR, Ríos-Gutiérrez M, Pérez P (2018) A molecular electron density theory study of the reactivity and selectivities in [3 + 2] cycloaddition reactions of C, N-Dialkyl nitrones with ethylene derivatives. J Org Chem 83(4):2182–2197. https://doi.org/10.1021/acs.joc.7b03093
5. Mohammad-Salim H, Hassan R, Abdallah HH, Oftadeh M (2020) The theoretical study on the mechanism of [3+2] cycloaddition reactions between α, β-unsaturated selenoaldehyde with nitrone and with nitrile oxide. J Mexican Chem Soc. https://doi.org/10.29356/jmcs.v64i2.1111
6. Domingo LR, Acharjee N (2020) Unravelling the strain-promoted [3+2] cycloaddition reactions of phenyl azide with cycloalkynes from the molecular electron density theory perspective. New J Chem 44(32):13633–13643. https://doi.org/10.1039/D0NJ02711A
7. Domingo LR, Acharjee N Unveiling the high reactivity of strained dibenzocyclooctyne in [3 + 2] cycloaddition reactions with diazoalkanes through the molecular electron density theory. J Phys Organ Chem. Doi: https://doi.org/10.1002/poc.4100
8. Domingo LR, Acharjee N (2020) A molecular electron density theory study of the Grignard reagent-mediated regioselective direct synthesis of 1,5-disubstituted-1,2,3-triazoles. J Phys Org Chem. https://doi.org/10.1002/poc.4062
9. Domingo LR, Ríos-Gutiérrez M, Acharjee N (2019) A molecular electron density theory study of the chemoselectivity, regioselectivity, and diastereofacial selectivity in the synthesis of an anticancer spiroisoxazoline derived from α-santonin. Molecules 24(5):832. https://doi.org/10.3390/molecules24050832
10. Abbiche K, MohammadSalim H, Salah M, Mazoir N, Zeroual A, Alaoui El, El Abdallaoui H, El Hammadi A, Hilali M, Abdallah HH, Hochlaf M (2020) Insights into the mechanism and regiochemistry of the 1,3-dipolar cycloaddition reaction between benzaldehyde and diazomethane. Theor Chem Acc 139(9):148. https://doi.org/10.1007/s00214-020-02662-4
11. Sato H, Kusumi T, Imaye K, Kakisawa H (1975) synthesis of 4-amino-2-hydroxybutyric acids. Chem Lett 4(9):965–966
12. Becke AD, Edgecombe KE (1990) A simple measure of electron localization in atomic and molecular systems. J Chem Phys 92(9):5397–5403. https://doi.org/10.1063/1.458517
13. Silvi B, Savin A (1994) Classification of chemical bonds based on topological analysis of electron localization functions. Nature 371(6499):683–686. https://doi.org/10.1038/371683a0
14. Geerlings P, De Proft F, Langenaeker W (2003) Conceptual density functional theory. Chem Rev 103(5):1793–1874. https://doi.org/10.1021/cr990029p
15. Domingo LR, Ríos-Gutiérrez M, Pérez P (2016) Applications of the conceptual density functional theory indices to organic chemistry reactivity. Molecules 21(6):748. https://doi.org/10.3390/molecules21060748
16. Sutcliffe BT (2006) The idea of a potential energy surface. Mol Phys 104(5–7):715–722. https://doi.org/10.1080/00268970500418059
17. Domingo LR (2014) A new C-C bond formation model based on the quantum chemical topology of electron density. RSC Adv 4(61):32415–32428. https://doi.org/10.1039/C4RA04280H
18. Thom R (1974) Stabilité Structurelle et Morphogenèse (Interéditions) 1972. THOM, R, Modèles Mathématiques de la Morphogenèse (Edi-tions 10–18)
19. Krokidis X, Silvi B, Alikhani ME (1998) Topological characterization of the isomerization mechanisms in XNO (X=H, Cl). Chem Phys Lett 292(1):35–45. https://doi.org/10.1016/S0009-2614(98)00650-2
20. Frisch M, Trucks G, Schlegel H, Scuseria G, Robb M, Cheeseman J, Scalmani G, Barone V, Petersson G, Nakatsuji H (2016) Gaussian 16. Gaussian, Inc., Wallingford, CT
21. Schlegel HB (1982) Optimization of equilibrium geometries and transition structures. J Comput Chem 3(2):214–218. https://doi.org/10.1002/jcc.540030212
22. Wiberg KB (1986) Ab initio molecular orbital theory by W. J. Hehre, L. Radom, P. v. R. Schleyer, and J. A. Pople, John Wiley, New York, 548pp. Price: $79.95 (1986). J Comput Chem 7:379–379. https://doi.org/10.1002/jcc.540070314
23. Dresler E, Kącka-Zych A, Kwiatkowska M, Jasiński R (2018) Regioselectivity, stereoselectivity, and molecular mechanism of [3 + 2] cycloaddition reactions between 2-methyl-1-nitroprop-1-ene and (Z)-C-aryl-N-phenylnitrones: a DFT computational study. J Mol Model 24(11):329. https://doi.org/10.1007/s00894-018-3861-y
24. Alnajjar RA, Jasiński R (2019) Competition between [2 + 1]- and [4 + 1]-cycloaddition mechanisms in reactions of conjugated nitroalkenes with dichlorocarbene in the light of a DFT computational study. J Mol Model 25(6):157. https://doi.org/10.1007/s00894-019-4006-7
25. Adjieufack AI, Ndassa IM, Mbadcam JK, Ríos-Gutiérrez M, Domingo LR (2016) Understanding the reaction mechanism of the Lewis acid (MgBr 2)-catalysed [3+2] cycloaddition reaction between C-methoxycarbonyl nitrone and 2-propen-1-ol: a DFT study. Theoret Chem Acc 136(1):5. https://doi.org/10.1007/s00214-016-2028-0
26. Mohammad-Salim HA, Acharjee N, Domingo LR, Abdallah HH (2020) A molecular electron density theory study for [3 + 2] cycloaddition reactions of 1-pyrroline-1-oxide with disubstituted acetylenes leading to bicyclic 4-isoxazolines. Int J Quantum Chem. https://doi.org/10.1002/qua.26503
27. Domingo LR, Acharjee N, Mohammad-Salim HA (2020) Understanding the reactivity of trimethylsilyldiazoalkanes participating in [3+ 2] cycloaddition reactions towards diethylfumarate with a molecular electron density theory perspective. Organics 1(1):3–18. https://doi.org/10.3390/org1010002
28. Mohammad-Salim HA, Abdallah HH, Maiyelvaganan KR, Prakash M, Hochlaf M (2020) Mechanistic study of the [2+2] cycloaddition reaction of cyclohexenone and its derivatives with vinyl acetate. Theor Chem Acc 139(2):19. https://doi.org/10.1007/s00214-019-2542-y
29. Mohammad Salim H, Abdallah H (2019) Theoretical study for the [2+2] cycloaddition reaction mechanism of ketenes and their derivatives. Orient J Chem 35:1550–1556. https://doi.org/10.13005/ojc/350512
30. Fukui K (1970) Formulation of the reaction coordinate. J Phys Chem 74(23):4161–4163. https://doi.org/10.1021/j100717a029
31. Gonzalez C, Schlegel HB (1990) Reaction path following in mass-weighted internal coordinates. J Phys Chem 94(14):5523–5527. https://doi.org/10.1021/j100377a021
32. Gonzalez C, Schlegel HB (1991) Improved algorithms for reaction path following: higher-order implicit algorithms. J Chem Phys 95(8):5853–5860. https://doi.org/10.1063/1.461606
33. Tomasi J, Persico M (1994) Molecular interactions in solution: an overview of methods based on continuous distributions of the solvent. Chem Rev 94(7):2027–2094. https://doi.org/10.1021/cr00031a013
34. Simkin BIAk, Sheĭkhet IIi (1995) Quantum chemical and statistical theory of solutions: a computational approach. Ellis Horwood,
35. Cossi M, Barone V, Cammi R, Tomasi J (1996) Ab initio study of solvated molecules: a new implementation of the polarizable continuum model. Chem Phys Lett 255(4):327–335. https://doi.org/10.1016/0009-2614(96)00349-1
36. Cancès E, Mennucci B, Tomasi J (1997) A new integral equation formalism for the polarizable continuum model: theoretical

background and applications to isotropic and anisotropic dielectrics. J Chem Phys 107(8):3032–3041. https://doi.org/10.1063/1.474659
37. Barone V, Cossi M, Tomasi J (1998) Geometry optimization of molecular structures in solution by the polarizable continuum model. J Comput Chem 19(4):404–417. https://doi.org/10.1002/(sici)1096-987x(199803)19:4%3c404::aid-jcc3%3e3.0.co;2-w
38. Reed AE, Weinstock RB, Weinhold F (1985) Natural population analysis. J Chem Phys 83(2):735–746. https://doi.org/10.1063/1.449486
39. Reed AE, Curtiss LA, Weinhold F (1988) Intermolecular interactions from a natural bond orbital, donor-acceptor viewpoint. Chem Rev 88(6):899–926. https://doi.org/10.1021/cr00088a005
40. Lu T, Chen F (2012) Multiwfn: a multifunctional wavefunction analyzer. J Comput Chem 33(5):580–592. https://doi.org/10.1002/jcc.22885
41. Humphrey W, Dalke A, Schulten K (1996) VMD: visual molecular dynamics. J Mol Graph 14(1):33–38. https://doi.org/10.1016/0263-7855(96)00018-5
42. Huisgen R (1976) 1,3-Dipolar cycloadditions. 76. Concerted nature of 1,3-dipolar cycloadditions and the question of diradical intermediates. J Organ Chem 41(3):403–419. https://doi.org/10.1021/jo00865a001
43. Parr RG, Yang W (1995) Density-functional theory of the electronic structure of molecules. Annu Rev Phys Chem 46(1):701–728. https://doi.org/10.1146/annurev.pc.46.100195.003413
44. Domingo LR, Ríos-Gutiérrez M, Duque-Noreña M, Chamorro E, Pérez P (2016) Understanding the carbenoid-type reactivity of nitrile ylides in [3+2] cycloaddition reactions towards electron-deficient ethylenes: a molecular electron density theory study. Theoret Chem Acc 135(7):160. https://doi.org/10.1007/s00214-016-1909-6
45. Domingo LR, Acharjee N (2018) [3+2] Cycloaddition reaction of C-phenyl-N-methyl nitrone to acyclic-olefin-bearing electron-donating substituent: a molecular electron density theory study. ChemistrySelect 3(28):8373–8380. https://doi.org/10.1002/slct.201801528
46. Acharjee N, Banerji A (2020) A molecular electron density theory study to understand the interplay of theory and experiment in nitrone-enone cycloaddition. J Chem Sci 132(1):65. https://doi.org/10.1007/s12039-020-01766-5
47. Domingo LR, Aurell MJ, Pérez P, Contreras R (2002) Quantitative characterization of the global electrophilicity power of common diene/dienophile pairs in Diels-Alder reactions. Tetrahedron 58(22):4417–4423. https://doi.org/10.1016/S0040-4020(02)00410-6
48. Jaramillo P, Domingo LR, Chamorro E, Pérez P (2008) A further exploration of a nucleophilicity index based on the gas-phase ionization potentials. J Mol Struct (Thoechem) 865(1):68–72. https://doi.org/10.1016/j.theochem.2008.06.022
49. Parr RG, Weitao Y (1994) Density-functional theory of atoms and molecules. Oxford University Press, Oxford
50. Parr RG, Pearson RG (1983) Absolute hardness: companion parameter to absolute electronegativity. J Am Chem Soc 105(26):7512–7516. https://doi.org/10.1021/ja00364a005
51. Parr RG, Lv S, Liu S (1999) Electrophilicity index. J Am Chem Soc 121(9):1922–1924. https://doi.org/10.1021/ja983494x
52. Domingo LR, Chamorro E, Pérez P (2008) Understanding the reactivity of captodative ethylenes in polar cycloaddition reactions. A theoretical study. J Org Chem 73(12):4615–4624. https://doi.org/10.1021/jo800572a
53. Benchouk W, Mekelleche SM, Silvi B, Aurell MJ, Domingo LR (2011) Understanding the kinetic solvent effects on the 1,3-dipolar cycloaddition of benzonitrile N-oxide: a DFT study. J Phys Org Chem 24(7):611–618. https://doi.org/10.1002/poc.1858
54. Domingo LR, Ríos-Gutiérrez M, Pérez P (2020) A molecular electron density theory study of the participation of tetrazines in aza-Diels–Alder reactions. RSC Adv 10(26):15394–15405. https://doi.org/10.1039/D0RA01548B